

# Movers and shakers: Granular damping in microgravity

M. N. Bannerman, J. E. Kollmer, A. Sack, M. Heckel, P. Mueller, and T. Pöschel

*Institute for Multiscale Simulation, Universität Erlangen-Nürnberg, Nügelnsbachstraße 49b, 91052 Erlangen, Germany*

(Dated: October 8, 2018)

The response of an oscillating granular damper to an initial perturbation is studied using experiments performed in microgravity and granular dynamics simulations. High-speed video and image processing techniques are used to extract experimental data. An inelastic hard sphere model is developed to perform simulations and the results are in excellent agreement with the experiments. The granular damper behaves like a frictional damper and a linear decay of the amplitude is observed. This is true even for the simulation model, where friction forces are absent. A simple expression is developed which predicts the optimal damping conditions for a given amplitude and is independent of the oscillation frequency and particle inelasticities.

PACS numbers: Valid PACS appear here

## I. INTRODUCTION

The characteristic property of dynamic granular systems, when compared to other many-particle systems, is their ability to dissipate mechanical energy through particle collisions. While the dissipative properties of vibrated granulate have long been investigated [1, 2], recently a large body of literature [3–8] has emerged on the mechanics and technical application of this damping mechanism in the form of *granular dampers*. A granular damper is a container partly filled by granular particles which may be attached to vibrating machinery to attenuate the amplitude of the oscillations. In its regime of operation, the granular material is in a gaseous state and its dynamics is determined primarily by the interparticle collisions rather than by long-lasting sliding contacts between the grains. *Static granular dampers* (e.g., Refs. [9, 10]) which exploit the rheology of granular matter and *impact dampers* (e.g., Refs. [11–14]), where only one or few particles are located in a cavity and dissipate energy in collisions with the walls of the container, are not considered here.

Granular dampers have a number of properties which are desirable in a wide range of technical applications: Unlike traditional dampers, granular dampers do not require an anchor in order to restrict the motion of the system. This is advantageous for damping in portable equipment and in space applications where no fixed anchor is available. Granular dampers are extremely simple devices consisting solely of particles enclosed in a container or cavity and require very little maintenance. Granular dampers do not suffer from significant aging when compared to the oil and rubber components of traditional dampers. Finally, granular dampers can operate over a wide range of temperatures without performance degradation as the mechanics of the particle-particle and particle-wall interactions exhibit only a weak dependence on the temperature. Modern technical applications of granular dampers include the damping of blade integrated disks (blisks) for compressors [15], structural vibration damping [16–18], noise reduction of bank note processing machines [19] and others. Perhaps the most common application is the *dead-blow hammer* [20] and in other impact damping handles [21].

The macroscopic damping properties of granular dampers under dynamic load is complicated, highly non-linear, and there is no straightforward way to optimize their performance

for a given situation. This has been demonstrated in a number of experiments and Molecular Dynamics (MD) simulations, including investigations on the attenuation of a free spring or cantilever with an attached granular damper [5, 7, 22–24]. The response of an oscillating cantilever with respect to periodic forcing has also been studied [25–30]. Even more complex systems have been investigated, such as the oscillation modes of a plate with an abundance of granulate filled cavities [31–34] with the aim of noise reduction [19]. For simple systems, such as cantilever oscillators, some progress has been made. Theoretical models have been developed based on phenomenological descriptions of the multiphase gas-particle flow of granular matter for attenuating oscillations [35] and also for driven steady state oscillations [36].

A granular damper, that is a dynamical system of dissipative interacting particles, obviously must be able to dissipate energy; however, its general behavior is not clear *á priori*. Properties, such as the dissipation rate, are complex functions of the frequency and amplitude of the oscillation, as well as the particle properties, the extension and characteristics of the container or cavities, and the filling fractions. More work is needed in this field to generate experimental results and corresponding models capable of describing the dynamics of granular dampers.

Saluena et al. [1] have shown that several regimes of energy dissipation exist for a granular damper and that the transitions between these regimes are determined primarily by the influence of gravity. An efficient operation of a granular damper can be expected only if the average kinetic energy of the particles is much larger than their average potential energy and the damper operates in the *dynamic or collisional regime*. In order to carefully investigate this regime, the influence of gravity should be minimized and experimental investigations should be performed under conditions of weightlessness.

The objective of this paper is to develop an effective model for the energy dissipation of a granular damper operating in the collisional regime. Our approach is as follows: First, experiments in microgravity are performed and the attenuation of a spring with an attached granular damper for several sets of parameters is obtained (Sec. II). A model capable of reproducing the experimental results is also developed and high-precision Discrete Element Method (DEM) simulations are performed (Sec. III). The two free parameters of

the model (inelasticities) are obtained by adjusting the values until the simulation matches the experiment as closely as possible for a single experiment (Sec. III C). From the excellent agreement of the simulation results for the fitted system and *for all other* experiments, it is concluded that the model underlying the simulation replicates the system’s essential features (Sec. III D). Thus, the DEM simulations are an effective model for granular damping in the collisional regime. In Sec. IV, a simple equation for the optimal design of a simple damper is derived and tested against the results of the DEM simulations. Section V discusses the observed linear decay of the amplitude and compares it to friction-damped oscillators. Finally, in Sec. VI the conclusions of the paper are outlined.

## II. EXPERIMENTAL SETUP

Figure 1 is a diagram of the experimental setup. Our granular damper comprises of a container of adjustable length which is partially filled with granular material. The damper is mounted to one end of a spring-steel blade and the opposite end is clamped in a solid aluminum base plate. The spring blade is described fully in Sec. III C. The rectangular damper container is constructed from 5 mm thick transparent polycarbonate plates. The internal dimensions of the container are  $50 \text{ mm} \times 50 \text{ mm} \times L$ , where the length  $L$  (in the direction of the oscillation) is adjusted by altering the spacing of the end walls. The container’s net weight (without granulate) is  $M = 434 \text{ g}$ . In this work, four different container lengths of  $L = 40, 65, 85,$  and  $104 \text{ mm}$  are used. The damper is loaded with 37 precision steel ball-bearings of diameter  $\sigma = 10 \text{ mm}$  and mass  $m = 4.04 \text{ g}$ . This number of particles is chosen as it packs to form a dense layer, two particles deep, on the end walls of the container.

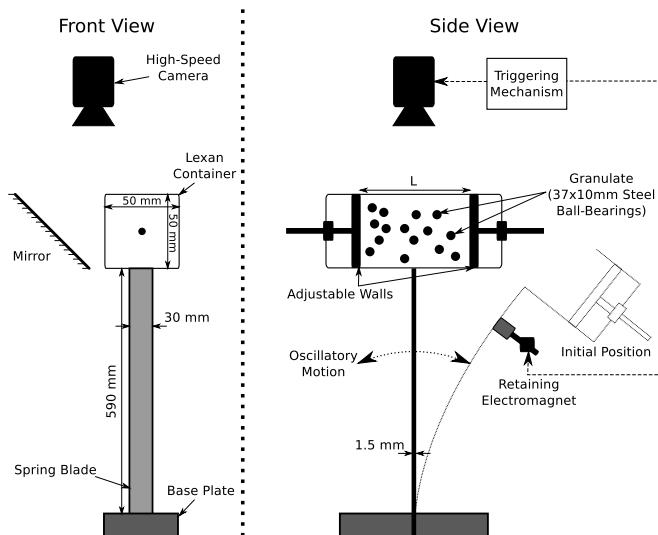


FIG. 1: Schematic of the experimental setup in front view (left) and side view (right). The curvature of the oscillations is exaggerated for the purpose of illustration.

The motion of the damper and contained granulate is

recorded using a high speed camera (MotionScope M3™), which records at a frame rate of 500 fps and with a spatial resolution of  $1024 \times 1280$  pixels. A  $45^\circ$  mirror is placed at the side of the container and allows for the simultaneous observation of the granulate from the top and the side. The position of the damper and the center of gravity of the particles are extracted from the top-view using standard image processing techniques. Although the side view facilitates more complex methods of reconstruction, it will be shown that the motion of the granulate is well described by the center of mass motion. All position measurements are made in a 2D plane which is parallel to and intersecting the top of the container while it is in its equilibrium position. Although this introduces some error at the peaks of the oscillations due to the curved damper trajectory, this error is negligible.

At the start of the experiment, the spring blade is deflected and held at the initial displacement of  $\Delta_0 = 107.5 \text{ mm}$  using an electromagnet. A trigger mechanism begins the experiment and starts the camera recording. After a short delay of 1 s, the spring blade is released from the electromagnet and the oscillations are recorded for 30 seconds.

To assure conditions of weightlessness, the experiment is performed on a modified Airbus A300 aircraft which has been retrofitted for performing parabolic flights. The parabolic flight provides a suitable microgravity environment ( $\pm 0.05 \text{ g}$ ) which lasts around 22 s and allows a number of experiments to be performed. In the following section, the numerical model and simulation techniques are described.

## III. NUMERICAL MODEL AND SIMULATION METHOD

A sufficiently complex model, capable of reproducing the observed experimental behavior, must be found if the system’s dynamics is to be understood. The model presented here is complex enough to yield quantitative agreement with the experiments and yet simple enough to gain insight into the dynamics of the system. The model for the granulate consists of a system of  $N$  smooth inelastic hard spheres, each of mass  $m$  and diameter  $\sigma$ . Although inelastic hard spheres are a basic model for the granulate they capture all of the essential behavior of the system: dissipative interactions between hard spherical particles. Friction forces, which typically play a large role in granular systems, are also neglected and the implications of this approximation are discussed later.

To model the oscillating mass and granular damper, the hard spheres are shaken in a rectangular box of mass  $M$ , which is coupled to a linear spring. The box is assumed to remain parallel to the axis of the system and oscillate along only one axis. By only permitting oscillations in a single dimension, this model neglects the arcing motion of the blade spring (see Fig. 1) and oscillatory modes induced by the collisions of the particles with the box; however, these effects are expected to be small in comparison to the dynamics of the modeled oscillation. With these approximations, the collision-free motion of the box can then be modeled using a simple

harmonic oscillator

$$\vec{r}_{\text{Box}}(t) = \hat{n} \Delta \cos[2\pi\omega(t + t_{\text{shift}})] + \vec{r}_{\text{Box}}^{(0)} \quad (1)$$

where  $\vec{r}_{\text{Box}}$  is the current position of the oscillator,  $\vec{r}_{\text{Box}}^{(0)}$  is its equilibrium position,  $\hat{n}$  is the unit vector in the direction of the oscillation, and  $\omega$  is the frequency of the empty damper. The amplitude of the oscillation  $\Delta$  and the phase shift of the oscillator  $t_{\text{shift}}$  are dynamical quantities and are altered by particle-box interactions. At time  $t = 0$ , the plate is at its positive maximum ( $t_{\text{shift}} = 0$ ) with an initial displacement of  $\Delta = \Delta_0$ .

The methods for performing event-driven simulations using smooth hard-spheres and fixed walls are well established (e.g., see Ref. [37]) and will not be discussed in detail. Here an event-driven dynamics simulation package (DYNAMO [38]) is used to simulate the dynamics of granular-damped oscillators. The only extension to the basic event-driven method concerns the detection and execution of events between particles and the oscillating boundary walls perpendicular to the oscillation direction  $\hat{n}$ , which is discussed in the following subsections.

### A. Detecting Oscillating Wall Interactions

Event-driven algorithms require an expression to calculate if and when a collision (an *event*) occurs between a particle and the bounding walls of the damper. If a collision is detected and it is the next event to occur in the system, the system is moved to the time of the collision and the event is executed by updating the velocities of the colliding particle, and the phase shift  $t_{\text{shift}}$  and amplitude  $\Delta$  of the oscillator.

To determine the time at which a particle  $i$  will collide with an oscillating wall, the equations of motion for the particle and the oscillating plate must be solved. Essentially, this is a search for the shortest positive root  $\Delta t$  of the function

$$f(\Delta t) = [\vec{r}_i + \Delta t \vec{v}_i - \vec{r}_{\text{Box}}(\Delta t + t)] \cdot \hat{n} \pm \left( \frac{L - \sigma}{2} \right) = 0 \quad (2)$$

where  $\vec{r}_i$  and  $\vec{v}_i$  are the position and velocity of particle  $i$  at the current system time  $t$ , and  $\Delta t$  is the time till collision. The sign of the term  $\pm(L - \sigma)/2$  is used to set which side of the oscillating box is tested for collisions.

To guarantee that no roots are missed, the root finding technique of Frenkel and Maguire [39] is used. This root finding routine requires a fixed interval to search for possible roots. The upper bound on the interval to search is determined from the time the freely moving particle takes to cross the extrema of the tested-wall's oscillation

$$\Delta t_{\text{max}} = \frac{\text{sgn}(\hat{n} \cdot \vec{v}_i) ([L - \sigma]/2 + \Delta) - \hat{n} \cdot (\vec{r}_i - \vec{r}_{\text{Box}}^{(0)})}{\hat{n} \cdot \vec{v}_i} \quad (3)$$

where  $\text{sgn}(x)$  is the sign function. The lower bound is typically the current system time ( $\Delta t_{\text{min}} = 0$ ); however, if the last

event to occur was a collision between this particle and a oscillating wall, the lower bound is increased to avoid re-detecting the same root. The lower bound is then set to

$$\Delta t_{\text{min}} = \frac{|2\dot{f}(0)|}{\dot{f}_{\text{max}}} \quad (4)$$

where  $\dot{f}_{\text{max}} = \Delta\omega^2$  is the maximum absolute second derivative of Eq. (2). The root finding technique used to search for suitable roots of Eq. (2) iterates towards a root from the boundaries of the interval by approximating the function at each iteration with a parabola. The equation of the parabola is generated using the derivatives of Eq. (2) and its smallest root provides the next iteration point. The iterations are halted on the  $n$ th iteration once the following criterion is met

$$|\Delta t_n - \Delta t_{n-1}| < \frac{[L - \sigma]}{2\dot{f}_{\text{max}}} \times 10^{-12} \quad (5)$$

where  $\dot{f}_{\text{max}} = |\vec{v}_i \cdot \hat{n}| + 2\pi\omega\Delta$  is the maximum absolute first derivative of Eq. (2). Unlike the hard line system of Frenkel and Maguire [39], all roots of Eq. (2) are acceptable and only the earliest root must be found. This completes the description of the collision detection and root finding technique.

### B. Executing Particle-Oscillating Wall Collisions

The final part of the simulation algorithm concerns the execution of oscillating boundary wall collisions. The conservation of momentum and the assumption of a constant coefficient of inelasticity leads to

$$\Delta \vec{p}_i = -\Delta \vec{p}_{\text{wall}} = -\mu(1 + \varepsilon_{\text{pw}}) \left( \hat{n} \cdot [\vec{v}_i - \dot{\vec{r}}_{\text{Box}}] \right) \hat{n} \quad (6)$$

where  $\Delta \vec{p}_i$  and  $\Delta \vec{p}_{\text{wall}}$  are the momentum change of the colliding particle  $i$  and oscillating wall respectively,  $\mu = mM/(m+M)$  is the relative mass, and  $\varepsilon_{\text{pw}}$  is the coefficient of inelasticity for particle-wall collisions. During a collision, the phase,  $t_{\text{shift}}$ , and amplitude,  $\Delta$ , of the oscillating wall are altered under the constraints of conserving momentum and the current box position. This results in the following expressions for the post collision state of the oscillating plate

$$t'_{\text{shift}} = \frac{1}{\omega} \arctan \left( \frac{-\hat{n} \cdot [\Delta \vec{p}_{\text{Box}} + \dot{\vec{r}}_{\text{Box}}]}{2\pi\omega\hat{n} \cdot [\vec{r}_{\text{Box}} - \vec{r}_{\text{Box}}^{(0)}]} \right) - t \quad (7)$$

$$\Delta' = \frac{\hat{n} \cdot (\vec{r}_{\text{Box}} - \vec{r}_{\text{Box}}^{(0)})}{\cos(2\pi\omega[t + t'_{\text{shift}}])} \quad (8)$$

where the primes denote post-collision values. Care must be taken at this point in the calculation to ensure that the magnitude of  $t$  and  $t_{\text{shift}}$  do not affect the precision of the calculations. Care must be taken also to retain the correct quadrant of the calculated angle when using the arctan function.

A difficulty with the event-driven simulation method arises from its inability to simulate events with finite durations.

When the oscillating wall is accelerating, a particle can repeatedly collide with the plate until its relative velocity and separation are numerically zero. Physically, the particle sticks to the wall and is pushed until the plate enters the deceleration phase of its oscillation, or interacts with another particle. To prevent this unresolvable situation from occurring within the event-driven simulation, the interactions between the oscillating wall and a particle are turned elastic when

$$\frac{\hat{n} \cdot (\vec{v}_i - \dot{\vec{r}}_{\text{Box}})}{\pi \omega \Delta} < 0.04 \quad (9)$$

The pushing of the particle is then transformed into a sequence of small hops which, as in the physical pushed case, do not dissipate energy. As this expression is linear in the current displacement  $\Delta$ , the long time behavior of the system is still recovered ( $\Delta \rightarrow 0$  as  $t \rightarrow \infty$ ). This elastic approximation is small when the plate motion dominates the dynamics of the system and the results appear to be unaffected if smaller values for Eq. (9) are used.

### C. Parameters of the Simulation

The simulations are initialized with all particles arranged in a regular lattice (FCC), with initial velocities assigned from a Gaussian and a total particle energy less than  $< 0.002\%$  of the initial spring energy. The particles are packed in a loose layer on the wall at the initial extrema of the oscillation. The particles in the experiment are also typically arranged this way due to the influence of gravity before the microgravity phase of the experiment.

The simulations require several inputs and these parameters are reported in Table I. All parameters, with the exception of the box frequency  $\omega$  and inelasticities  $\varepsilon_{pp}$  and  $\varepsilon_{pw}$ , are directly obtained from the experimental setup described in Sec. II. The three remaining parameters must be calculated from material parameters or obtained through experimental results.

TABLE I: Model parameters for the event-driven simulations.

$\sigma$ (mm)	$m$ (g)	$N$	$\Delta_0$ (mm)	$\omega$ ( $s^{-1}$ )	$M$ (g)	$\varepsilon_{pp}$	$\varepsilon_{pw}$
10	4.04	37	107.5	1.23	434	0.75	0.76

The frequency of the unloaded damper  $\omega$  may be estimated using the simple harmonic oscillator model. The spring constant of the spring-blade may be calculated using the Euler-Bernoulli beam equation

$$k = \frac{E w h^3}{4 l^3} = 0.0254 \text{ N mm}^{-1} \quad (10)$$

where  $E = 2.06 \times 10^5 \text{ N mm}^{-2}$  is the elastic modulus of the spring steel,  $w = 30 \text{ mm}$  is the spring width,  $h = 1.5 \text{ mm}$  is the spring thickness, and  $l = 590 \text{ mm}$  is the spring length. If the system behaves as a simple harmonic oscillator and the

mass of the spring is ignored the frequency may be estimated using

$$\omega \approx \frac{1}{2\pi} \sqrt{\frac{k}{M}} \approx 1.217 \text{ s}^{-1} \quad (11)$$

The frequency of the loaded granular damper ( $\omega_{\text{system}}$ ) is lower than that of the empty damper ( $\omega$ ) due to the added mass and the interactions of the granulate. In the simple harmonic oscillator model, the additional mass of the granulate alters the frequency of the oscillations by

$$\omega_{\text{loaded}} = \omega \sqrt{\frac{M}{M + N m}} \quad (12)$$

In the limit that the granulate is tightly packed in the granular damper, the frequency of the system should limit to the simple harmonic oscillator frequency  $\omega_{\text{system}} \rightarrow \omega_{\text{loaded}}$ . In the limit of a large box, the granulate will completely decouple from the oscillator and  $\omega_{\text{system}} \rightarrow \omega$ . Remarkably, the frequency of the experimental oscillators, obtained through averaging the peak and center point frequencies, is consistent for all box lengths at approximately  $\omega_{\text{system}} \approx 1.05 \text{ s}^{-1}$  with a standard deviation of  $\pm 0.01 \text{ s}^{-1}$ . If it is assumed that  $\omega_{\text{system}} \approx \omega_{\text{loaded}}$  for small box lengths, Eq. (12) estimates an unloaded frequency of  $\omega \approx 1.22 \pm 0.1 \text{ s}^{-1}$  for the experimental system. This agreement with the beam equation is promising and suggests that, although the granulate is periodically decoupled from the oscillator, the deviation from Eq. (12) is still small for the experimental box lengths studied here. For the simulations, a slightly higher frequency of  $\omega \approx 1.23 \text{ s}^{-1}$  is used which is within the standard deviation of the experimental values and yields an excellent fit to the experimental data.

Finally, the coefficients of restitution  $\varepsilon_{pp}$  and  $\varepsilon_{pw}$  describing the inelastic collisions between particles and between a particle and the wall must be determined. These model parameters are obtained by fitting simulation results to the experimental data for the smallest box length ( $L = 40 \text{ mm}$ , Fig. 2). As best fits the following results are obtained

$$\varepsilon_{pp} = 0.75 \quad \varepsilon_{pw} = 0.76 \quad (13)$$

The value for the particle-wall coefficient of restitution is in close agreement with published results reported for a 9.35mm steel ball-bearing impacting a clamped acrylic plate [40]; however, the particle-particle inelastic coefficient is significantly lower than expected. Performing an automated drop test [41] of the granulate on to a silicon carbide plate yields an elasticity of  $\varepsilon \approx 0.95$ . Due to the high rigidity of the base plate, this value should be close to the experimental value for particle-particle interactions. The fitted particle-particle inelasticity  $\varepsilon_{pp}$  may be unexpectedly lower than the drop test results due to missing dissipation mechanisms in the model (e.g., granulate friction). Despite this, the agreement of the simulation and experimental results (see Sec. III D) shows that this is still an effective model for the system.

It should be noted that the optimization/fitting of the inelasticities  $\varepsilon_{pp}$  and  $\varepsilon_{pw}$  is performed exclusively for the box

width of  $L = 40$  mm. For all other simulations reported here, the optimal coefficients of restitution are used without further fitting.

#### D. Validation of the Numerical Method

The simulation and experimental results are compared in this section to validate the model. Figure 2 presents the box position  $x_{\text{Box}}$  and granulate center of mass  $x_{\text{COM}}$  as a function of time for a box length of  $L = 40$  mm. Two experimental measurements are reported and both are in close agreement with the simulation results. The experimental and simulation results display a high degree of repeatability and single realizations are representative of the averaged values. This is due to the uniqueness of the initial state, with the spring held in a deflected state and the particles resting in a regular, repeatable layer on the outer wall due to the influence of gravity before the microgravity phase. However, the experimental results begin to fluctuate towards the end of the microgravity phase due to disturbances in the flight.

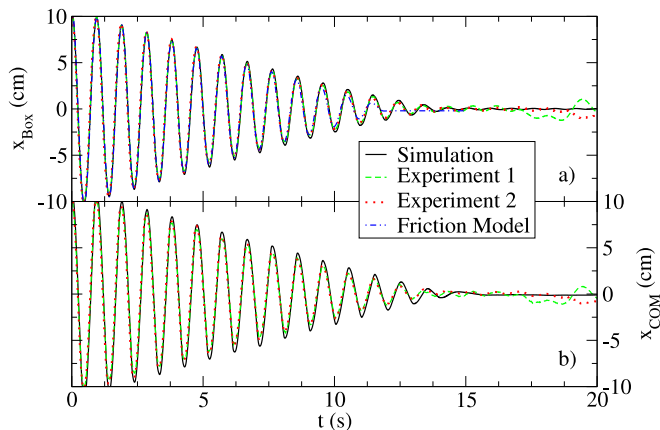


FIG. 2: (Color online) A comparison of simulation results, experimental data and Eq. (17) for (a) the box position  $x_{\text{Box}}$  and (b) the granulate center of mass  $x_{\text{COM}}$  as a function of time for a box length of  $L = 40$  mm. The simulation data is fitted to the experimental data through the inelasticities  $\varepsilon_{\text{pp}} = 0.75$  and  $\varepsilon_{\text{pw}} = 0.76$ .

The numerical result for the box position  $x_{\text{Box}}$  as a function of time is in excellent quantitative agreement with the experimental data. For the position of the center of mass,  $x_{\text{COM}}$  the agreement is also very good albeit not as close as for  $x_{\text{Box}}(t)$ , with some over-estimations near the peaks of the oscillations. The error could arise from the experimental method due to the top-down view of the simulation and 2D image reconstruction used. The area of the visible particles are identified and the centroid location is taken to be the center of mass. Due to the end walls and slight arcing motion of the box (see Fig. 1) the reconstructed center of mass is slightly biased towards the center of the box.

The agreement between the simulation and experiment for the frequency of the damped oscillator is excellent and confirms the accuracy of the fundamental frequency  $\omega$ ; however,

the excellent agreement in the amplitudes between experimental data and simulations for  $L = 40$  mm is perhaps not too surprising since this experimental data set is used to determine the coefficients of restitution,  $\varepsilon_{\text{pp}}$  and  $\varepsilon_{\text{pw}}$ . The model parameters are now fixed and the numerical result for several different box widths are compared with the corresponding experimental data (see Figs. 3-5).

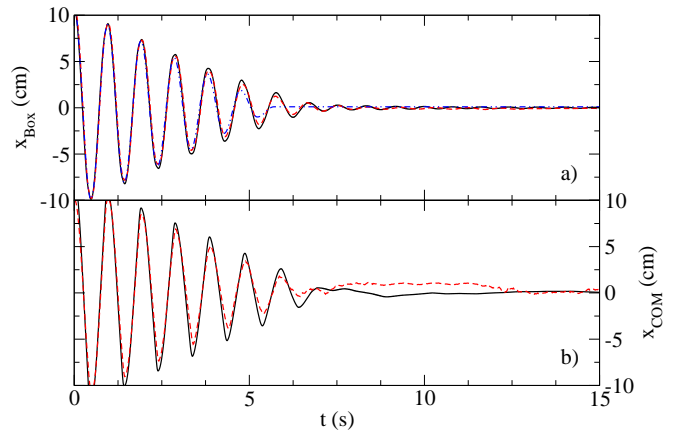


FIG. 3: (Color online) A comparison of simulation results, experimental data and Eq. (17) for (a) the box position  $x_{\text{Box}}$  and (b) the granulate center of mass  $x_{\text{COM}}$  as a function of time for a box length of  $L = 40$  mm. Line types are described in Fig. 2. The simulation data is not fitted to the experiment and the parameters of Fig. 2 are used.

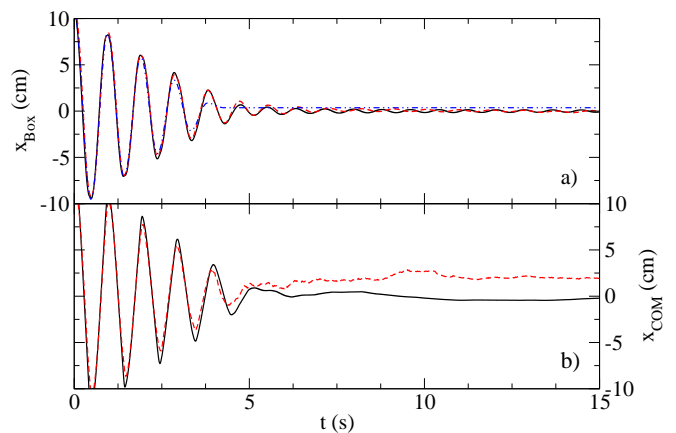


FIG. 4: (Color online) The same comparison as Fig. 3, but for a box length of  $L = 85$  mm.

In general, the simulation results are in excellent agreement with the models predictions. This implies that the approximations of the model (1 D oscillations, no air resistance, ideal spring) are small and have little effect on the dynamics of the granular damper. Some of these approximations may already be compensated for in the fitting of the coefficients of restitution, but they appear to be well behaved with the changes in box length. In the simulation, rotational degrees of freedom are neglected by eliminating friction between the particles and the particles and the container walls. In contrast to

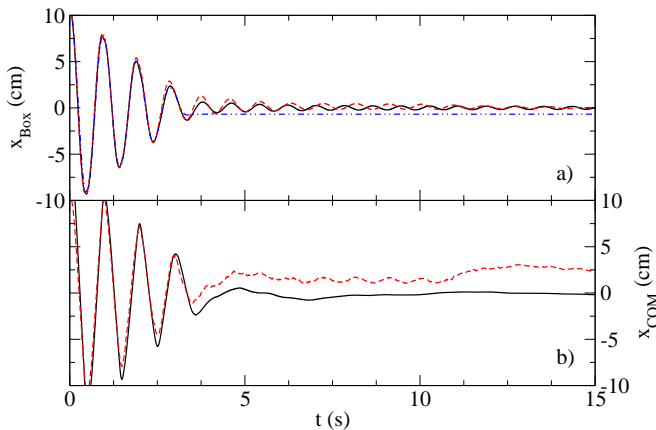


FIG. 5: (Color online) The same comparison as Fig. 3, but for a box length of  $L = 104$  mm.

vibrated granular dampers in gravity, where the energy dissipation due to friction is of the same scale as energy dissipation by impact [42], in microgravity friction seems to be less important or easily characterized into the restitution coefficient  $\varepsilon_{pp}$ . Overall, the fitting of the inelasticities appears to be effective at capturing the behavior of the system and no further parameters or extensions of the simulation model are required.

The most striking feature of the curves in Figs. 2-5 is the linear decay of the peak amplitude of the oscillation with time. A detailed discussion of this property is postponed to Sec. V and optimal dampers are discussed in the following section.

#### IV. OPTIMAL DAMPERS

There is a significant dependence of the damping efficiency on the container length, as is seen in Figs. 2–5. The number of cycles before the oscillations are sufficiently damped varies from 13 to 4 as the box length is increased. By examining the energy transfer mechanisms within the granular damper, an expression for optimizing the dampers design may be found.

Figure 6 plots the cumulative energy lost through the three classes of collisions in the simulation system. It should be noted that Fig. 6 is only valid for the fitted inelasticities and will therefore differ from the true experimental values. Nevertheless, the results should agree qualitatively and allow some insight into the experimental system. The sides of the box appear to be unimportant in this design of a damper and may present an opportunity for optimization by utilizing alternative shaker geometries (e.g., an hourglass design). Not only are the particle-end wall collisions the sole mechanism for the transfer of oscillation energy from the oscillator into the contained granulate, but simulation results estimate that these collisions are also a significant dissipation mechanism for the damper. The end wall interactions both transfer and dissipate the maximum energy when the relative velocity of the oscillator end walls and granulate are maximized. Therefore, maximizing this relative speed should optimize the performance of the granular damper. In the following subsection, an attempt is

made to estimate the optimal box length using a simple model for the dynamics.

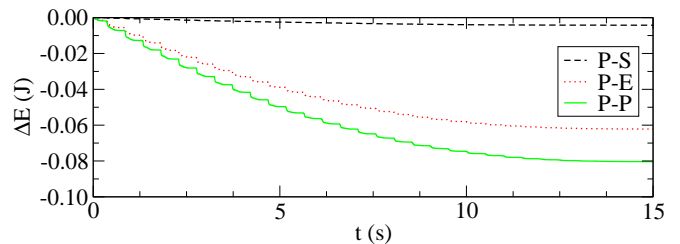


FIG. 6: (Color online) Simulation values for the cumulative energy loss through interactions with the side walls (P-S), end walls (P-E) and particle-particle interactions (P-P) for a box length of  $L = 40$  mm.

#### A. Theoretical Predictions

Attempting to optimize the system by modeling the granulate as a single particle or some other simplified description is difficult [43] due to the lack of an analytical solution to Eq. (2). To estimate the optimal damping conditions, only two plausible assumptions for the motion of the granulate in the box are required: a) the granulate will be “collected” and form a packed layer on the approaching oscillating wall during the initial inward stroke (when the oscillator accelerates towards the center point), and b) the center of mass velocity of the granulate at the end of the inward stroke is, on average, the maximum oscillator velocity. The time from the center of the stroke at which the granulate would hit the peak displacement of the oscillator is then given by

$$t_{g,\text{peak}} = \frac{L + \Delta - \sigma_{\text{layer}}}{2\pi\omega_{\text{loaded}}\Delta} \quad (14)$$

where  $\sigma_{\text{layer}} = 20$  mm is the thickness of the layer of granulate when it is packed on the surface of the oscillating wall. It should be noted that Eq. (14) decreases in time, as  $\Delta$  decreases on average due to interactions with the granulate. If for any integer  $n$  the peak collision time lies in the range  $n < \omega t_{g,\text{peak}} < n + 1/4$ , the granulate will hit the oscillating wall on the outward phase of its stroke. All experimental box with the exception of the largest system ( $L = 104$  mm) are within this regime. It is expected that improved damping occurs if the granulate hits on the inward stroke as the relative velocity is maximized.

The granulate travels the length of the box in

$$t_{g,\text{Box}} = \frac{L - \sigma_{\text{layer}}}{2\pi\omega_{\text{loaded}}\Delta} \quad (15)$$

If  $n + 1/4 > \omega t_{g,\text{peak}} > n + 1$  and  $n < \omega t_{g,\text{Box}} < n + 1/2$ , the granulate will collide on the inward phase of the stroke. The largest system, where  $\omega t_{g,\text{Box}} \approx 0.15$ , collides after the turning point of the oscillator; however, the dissipation is maximized when  $\omega t_{g,\text{Box}} \approx 1/2$ . At this point, the relative velocity

between the granulate and oscillating box is also maximized. For  $\omega t_{g, \text{Box}} > 1/2$  the plate is either decelerating or multiple cycles of the oscillation occur without the granulate colliding.

The damping of the oscillator from the initial state can be optimized, independently of the inelastic coefficients, by altering either  $L$ ,  $\omega$ , or  $\Delta$  such that  $\omega t_{g, \text{Box}} \approx 1/2$ . Efficiency will be lost and recovered as  $\Delta$  changes over time, but if the granulate is relatively inelastic this will occur after most of the energy is dissipated or transferred in the first cycle.

Setting  $\omega t_{g, \text{Box}} = 1/2$  in Eq. (15) and using Eq. (12), the optimal box length  $L_{\text{opt}}$  may be estimated for a given initial amplitude  $\Delta_0$  using

$$L_{\text{opt}} = \pi \Delta_0 \sqrt{\frac{M}{M + N m}} + \sigma_{\text{layer}} \quad (16)$$

This expression is remarkable in that it is independent of the oscillation frequency. This may be understood from dimensional analysis as, due to the negligible initial kinetic energy, the model has only one time scale. As such, the solutions to the model must scale trivially in the frequency of the oscillations. In the following subsection, the results of Eq. (16) and its assumptions are checked against simulation results.

### B. Numerical Test

The validity of the basic assumptions made in Sec. IV A and the result, Eq. (16), are now tested using the results of the DEM simulations. Using Eq. (16) to predict the optimal box length for the damping of the experimental system yields a value of  $L_{\text{opt}} = 311$  mm. The results of a simulation at this box length are presented in Fig. 7. A square step in the granulate center of mass velocity is visible at the peak of the box velocity as the granulate decouples from the oscillator. The assumption of an equal box and granulate velocity at the midpoint of the stroke (at peak velocity) appears to hold. Visual inspection [44] confirms the granulate is collected in a layer on the approaching oscillating wall. The re-collision of the granulate also appears to occur close to the peak of the box velocity, maximizing the relative velocity, energy dissipation, and energy transfer in this first collision. The largest oscillations are effectively damped within one second; however, the oscillator is now susceptible to smaller amplitude oscillations which appear to decay very slowly. The optimal approach would be to couple two or more dampers to damp a wider range of amplitudes within short timescales. This idea has already been pursued for impact dampers (e.g., Ref. [45]) which are related to granular dampers except that in the container or cavity there is only a single particle.

To test the predictions of Eq. (16) for the optimal damping length  $L$ , a suitable metric must be defined to compare various box lengths. Figure 8 compares the time an oscillator takes to dissipate a certain fraction of the initial energy as a function of the box length. Despite the continuing low-amplitude oscillations of the damper at  $L = 311$  mm (see Fig. 7), the damper effectively eliminates 95% of the initial energy in well under two oscillations. Equation (16) appears to yield an excellent estimate for the global optimal box length, avoiding both the

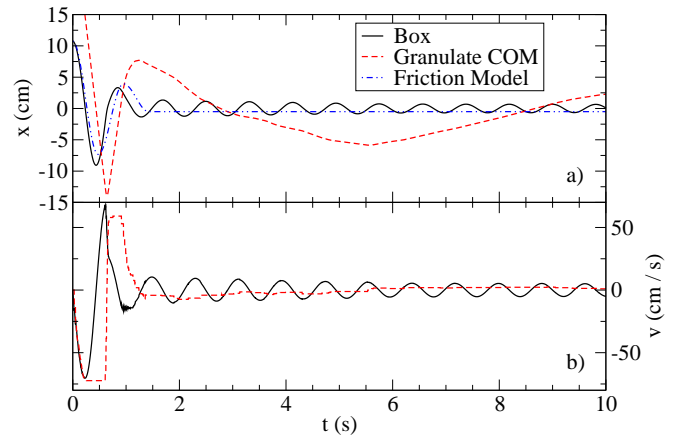


FIG. 7: (Color online) A comparison of simulation results, experimental data and Eq. (17) for the box and granulate (a) position, and (b) velocity as a function of time for the optimal box length of  $L = 311$  mm, as predicted by Eq. (16).

highly inefficient zones towards the edges of the graph. Previous work on forced granular dampers (e.g., see Fig. 7 in Ref. [25]) also yields performance curves with the same general U-shape as Fig. 8. An alternative metric for comparing

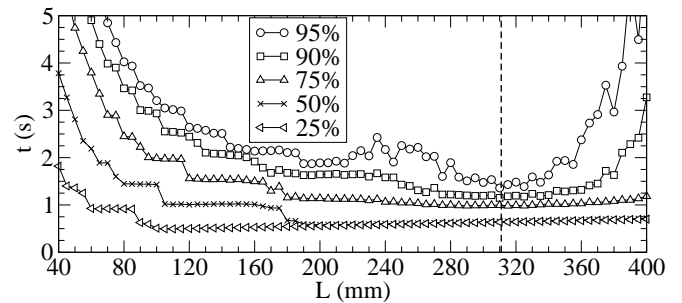


FIG. 8: Simulation results for the time  $t$  to dissipate a percentage of the initial energy, versus the box length  $L$ . The vertical dashed line indicates the optimal box length as predicted by Eq. (16).

the efficiency of granular dampers is now defined through a phenomenological model for the damping behavior.

### V. PHENOMENOLOGICAL MODEL OF GRANULAR DAMPERS

Figures 2–5 reveal a linear decay of the amplitude of the oscillation with time, and thus the energy of the system decays quadratically in time. This is highlighted in Fig. 9, where the time dependence of the square root of the total energy of the damper is plotted. This result is surprising considering the approximations of the previous section: the oscillator appears to have a constant frequency for a given box length, and the oscillator collects the granulate on a wall and then collides the granulate in each half period. For the amplitude decay to be linear, the energy dissipated in each of these “collisions” of the

granulate must then be proportional to the amplitude  $\Delta$ . However, if an inelastic particle is given a velocity proportional to the maximum plate velocity ( $2\pi\omega\Delta$ ), it will dissipate energy proportional to the square of the plate amplitude ( $\Delta^2$ ) for a given number of collisions.

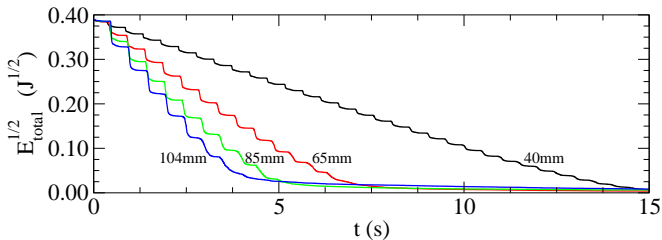


FIG. 9: (Color online) Total energies of the oscillators as obtained from numerical simulations.

The result is also surprising as the more common viscous dampers yield an exponential decay of the amplitude; however, the only simple damped-oscillator which displays a linear decay in the amplitude is one damped by a constant magnitude force [46] (e.g., a friction-damped oscillator). The equation of motion for such an oscillator is

$$M_{\text{tot}} \ddot{x} = -kx - \mu M_{\text{tot}} \text{sgn}(\dot{x}) \quad (17)$$

where  $x$  is the oscillator position,  $M_{\text{tot}} = M + Nm$  is the total oscillating mass and  $\mu M_{\text{tot}}$  is the magnitude of the constant frictional force. No simple analytical solution exists to this equation although piecewise solutions may be found [46]. This model does not appear to be appropriate for the granular damper due to the intermittent nature of the damping force. For example, the steps in the damper energy (Fig. 9) arise from the decoupling of the damping granulate and oscillator at the midpoint of the stroke (see Fig. 7) and during these steps the oscillator experiences no damping force. However, this model may still be useful in characterizing and comparing the damping efficiencies of granular dampers in microgravity through the effective frictional force  $\mu M_{\text{tot}}$ .

The effective frictional force of a experimental damper may be estimated through the decay of the peak amplitude, as given by

$$\mu M_{\text{tot}} = \frac{k(\Delta_0 - |x_n|)}{2n + 1 - (-1)^{2n}} \quad (18)$$

where  $n$  is the index of the amplitude peak and  $|x_n|$  is the absolute oscillator displacement for the  $n$ th peak. The peak number  $n$ , used to calculate the effective friction coefficient, should be odd to only sample the amplitude during the “collection” phase of the oscillation and should be as small as possible for correct measurement of rapid dampers. The earliest value of  $n$  which satisfies these requirements is  $n = 3$ , at a time of  $t = 1.5/\omega_{\text{system}}$ . Equation (18) is used to extract an effective friction force for each experimental system and the corresponding solutions to Eq. (17) are plotted in Figs. 2–5. For the non-optimal dampers the model fits the data well. Deviations begin to appear towards the end of the oscillations as the “collect and collide” motion begins to break down and the

granulate spreads uniformly over the box. This lends weight to the argument that the “collect and collide” motion of the granulate is responsible for the apparent friction-damped behavior. For the optimal damper (see Fig. 7), the model does not fit as well. The discrepancy arises from the oscillators frequency for this box length being significantly different from the predictions of Eq. 12. Simple spring models will no longer work and appear to be constrained to the range ( $t_{g,\text{peak}} \lesssim 1/4$ ). A better fit may be obtained by fitting the spring coefficient  $k$ , however this is unsatisfactory as the results of the model cannot be compared between systems. Another deficiency of the friction model is that it predicts that the damper will come to a complete halt after a finite time. It fails to capture the persistent small amplitude oscillations (see Fig. 7). The friction deceleration,  $\mu$ , still appears to be a useful value for comparing the damping efficiency of sub-optimal granular dampers.

The quadratic decay of energy with time in a granular system attached to a linear spring has been reported before [7, 23, 24, 47]. Surprisingly, the same behavior is found also for rather different dampers such as thrust-based damping [48] and impact dampers [49–52]. However, this is not a general rule and other published results exist (e.g., Ref. [5]) where a non-linear decay of the amplitude of the oscillation (possibly exponential) is found. This work clarifies that this apparent frictional behavior may also arise solely from the collisional granular dynamics and does not necessarily arise from friction forces within the experimental setup. This is evident as the simple model used in the simulations reproduces the linear decay of the amplitude.

## VI. CONCLUSIONS

In this paper, a method for performing controlled experiments on granular damped oscillators in microgravity is outlined. High-speed video capture and image-processing techniques are used to reconstruct the motion of the oscillator to obtain accurate experimental results. A simple hard sphere model and event-driven dynamics are also used to generate quantitative results that compare well against the experimental values. From the excellent agreement of the simulation and experimental frequency, it appears that the damper frequency responds like a simple harmonic oscillator to changes in load (Eq. (12)) for short box lengths. This is remarkable given the periodic decoupling of the granulate from the spring and box. The simulation model scales trivially with the frequency of the oscillations as, apart from the negligible initial energy, the model has only one time scale. Further research is required on experimental systems to determine the frequency dependence of granular dampers and generalize the current model to these systems.

The straightforward design of these granular dampers yields a remarkably simple expression for the optimal damping configuration of the form of Eq. (16). Simulations at the predicted optimal box length damp large amplitude oscillations remarkably well (see Fig. 7) but are susceptible to smaller amplitude disturbances. The final expression for the optimal box length is independent of the oscillation frequency,

which may be understood through dimensional analysis of the model.

Unlike conventional viscous-damped systems, the granular damped system studied here displays a linear decay in the amplitude. This behavior is not intuitive and is a feature typical of friction-damped oscillators. The simulation results and their excellent agreement with experimental results strongly suggest that this effect arises solely from the granular dynamics. The linear decay is a useful property as it implies that a granular damper can completely damp oscillations within a finite time; however, this is not the case as, at low oscillation energies a transition occurs and the damping force is significantly reduced. Further research is required in designing dampers with a wider amplitude response by coupling multiple dampers with different lengths. The internal geometries

may also be optimized to eliminate the decoupling of the granulate in the midpoint of the stroke to create more effective dampers.

### Acknowledgments

The authors would like to acknowledge the German Science Foundation (DFG) for funding via the grant SP608 and DLR for funding the parabolic flight campaign. Thanks also go to the mechanical workshop NW2 at the University of Bayreuth. Finally, the authors would like to acknowledge the additional funding of the DFG through the Cluster of Excellence Engineering of Advanced Materials in Erlangen.

- 
- [1] C. Saluena, T. Pöschel, and S. E. Esipov, *Phys. Rev. E* **59**, 4422 (1999).
- [2] C. Saluena, S. E. Esipov, T. Pöschel, and S. Simonian, *SPIE* **3327**, 23 (1998).
- [3] K. Mao, M. Wang, Z. Xu, and T. Chen, *J. Vib. Acoust.* **126**, 202 (2004).
- [4] K. Mao, Z. Xu, M. Wang, and T. Chen, in *Proc. IMPLAST* (2003), pp. 994–1005.
- [5] K. Mao, M. Y. Wang, Z. Xu, and T. Chen, *Powder Tech.* **142**, 154 (2004).
- [6] C. Tianning, K. Mao, H. Xieqing, and M. Wang, *SPIE* **4331**, 294 (2001).
- [7] X.-M. Bai, L. M. Keer, Q. J. Wang, and R. Q. Snurr, *Gran. Matt.* **11**, 417 (2009).
- [8] X.-M. Bai, B. Shah, L. M. Keer, Q. J. Wang, and R. Q. Snurr, *Powder Tech.* **189**, 115 (2008).
- [9] J. Bourinet and D. Houédec, *Computers & Structures* **73**, 395 (1999).
- [10] K. Cowden, D. Bishop, D. Walrath, and J. McInroy, *SPIE* **5052**, 317 (2003).
- [11] C. Cempel, *J. Sound Vib.* **40**, 249 (1975).
- [12] S. F. Masri, *J. Acoust. Soc. Am.* **47**, 229 (1970).
- [13] S. F. Masri, *J. Acoust. Soc. Am.* **45**, 1111 (1969).
- [14] M. Duncan, C. Wassgren, and C. Kroussgrill, *J. Sound Vib.* **286**, 123 (2005).
- [15] R. Kielb, F. G. Macri, D. Oeth, A. D. Nashi, P. Macioce, H. Panossian, and F. Lieghley, in *Proc. Nat. Turbine Engine High Cycle Fatigue Conf.* (1999).
- [16] H. V. Panossian, *J. Vibr. Acoust.* **114**, 101 (1992).
- [17] C. Cempel and G. Lotz, *J. Struct. Engrg.* **119**, 2624 (1993).
- [18] J. R. Fricke, *Sound and Vibration* **34**, 22 (2000).
- [19] Z. W. Xu, M. Y. Wang, and T. N. Chen, *J. Sound Vib.* **270**, 1033 (2004).
- [20] J. C. Norcross, *Dead-blow hammer head*, US Patent 3343576 (1967).
- [21] S. Ashley, *Mechanical Engineering* **117**, 80 (1995).
- [22] V. Kinra, K. Marhadi, and B. Witt, in *46th AIAA/ASME/ASCE/AHS/ASC Structures, Structural Dynamics, and Materials Conference* (2005), vol. 9, pp. 6376–6382.
- [23] K. S. Marhadi, Master's thesis, Texas A&M University (2003).
- [24] R. Friend and V. Kinra, *J. Sound Vib.* **233**, 93 (2000).
- [25] M. Saeki, *J. Sound Vib.* **251**, 153 (2002).
- [26] M. Saeki, *J. Sound Vib.* **281**, 1133 (2005).
- [27] B. Fowler, E. Flint, and S. Olson, *Proc. SPIE* **3989**, 356 (2000).
- [28] B. L. Fowler, E. M. Flint, and S. E. Olsen, *Proc. SPIE* **4331**, 186 (2001).
- [29] A. Papalou and S. Masri, *J. Vibration and Control* **4**, 361 (1998).
- [30] C. X. Wong, M. C. Daniel, and J. A. Rongong, *J. Sound Vib.* **319**, 91 (2009).
- [31] Z. W. Xu, M. Y. Wang, and T. N. Chen, *J. Vib. Acoust.* **126**, 141 (2004).
- [32] Z. W. Xu, M. Y. Wang, and T. N. Chen, *J. Sound Vib.* **279**, 1097 (2005).
- [33] J. Park and D. L. Palumbo, *Exp. Mech.* **49**, 697 (2009).
- [34] B. L. Fowler, Tech. Rep. A771024, Air Force Research Laboratory (2003).
- [35] C. Wu, W. Liao, and M. Wang, *J. Vib. and Acoust.* **126**, 196 (2004).
- [36] X. Fang and J. Tang, *J. Vib. Acoust.* **128**, 489 (2006).
- [37] T. Pöschel and T. Schwager, *Computational Granular Dynamics* (Springer, New York, 2005).
- [38] M. Bannerman, R. Sargant, and L. Lue (2009), arXiv:1004.3501v1.
- [39] D. Frenkel and J. F. Maguire, *Mol. Phys.* **49**, 503 (1983).
- [40] R. Sondergaard, K. Chaney, and C. E. Brennen, *J. Appl. Mech.* **57**, 694 (1990).
- [41] M. Montaine, M. Heckel, C. Kruelle, T. Schwager, and T. Pöschel, (in preparation).
- [42] T. Chen, K. Mao, X. Huang, and M. Y. Wang, *Proc. SPIE* **4331**, 294 (2001).
- [43] N. Popplewell and M. Liao, *J. Sound Vib.* **146**, 519 (1991).
- [44] See EPAPS Document No. [number will be inserted by publisher] for a slow-motion (16×) video comparing the simulation and experiment for a box length of  $L = 40$  mm.
- [45] S. F. Masri, *J. Acoust. Soc. Am.* **45**, 1111 (1969).
- [46] R. C. Hudson and C. R. Finfgeld, *Am. J. Phys.* **39**, 568 (1971).
- [47] K. S. Marhadi and V. K. Kinra, *J. Sound Vib.* **283**, 433 (2005).
- [48] B. M. Shah, D. Pillet, X.-M. Bai, L. M. Keer, Q. J. Wang, and R. Q. Snurr, *J. Sound and Vib.* **326**, 489 (2009).
- [49] W. M. Mansour and D. R. T. Filho, *J. Sound Vib.* **33**, 247 (1974).
- [50] M. Y. Yang, G. H. Koopmann, G. A. Lesieutre, and S. A. Hambric, in *ASME Conf. Proc.* (2002), pp. 113–118.
- [51] C. C. Cheng and J. Y. Wang, *Int. J. Mech. Sci.* **45**, 589 (2003).
- [52] Y. Du, S. Wang, Y. Zhu, L. Li, and G. Han, *Adv. Acoust. Vibr.* **2008**, 140894 (2008).